



 Cite this: *RSC Adv.*, 2020, 10, 42200

 Received 19th October 2020  
Accepted 12th November 2020

DOI: 10.1039/d0ra08892g

rsc.li/rsc-advances

# Irregular solution thermodynamics of wood pulp in the superbase ionic liquid [m-TBDH][AcO]<sup>†</sup>

 Gordon W. Driver \* and Ilkka A. Kilpeläinen

Knowledge of solution thermodynamics is fundamental for solution control and solvent selection processes. Herein, experimentally determined thermodynamic quantities for solutions of wood pulp (hardwood dissolving pulp, *i.e.* cellulose) in [m-TBDH][AcO] are presented. *Model-free* activities ( $a_{i,j}$ ) and associated *mass fraction* ( $w_{i,j}$ ) activity coefficients ( $\Omega_{i,j}$ ), are determined to quantify inherent solution *non-ideality*. Access to the Gibbs energy of mixing,  $G_{\text{mix}}$ , in combination with associated partial molar thermodynamic quantities, reveal strong enthalpically favourable (exothermic) interactions due to solvent-*j* and solute-*i* contact-encounters. Onset of an entropy driven phase instability appears at increased temperatures as excess entropic contributions dominate solvation character of the *irregular* solutions formed.

Investigations concerning dissolution of carbon-neutral biomass components in varieties of ionic liquids (ILs) have increasingly populated the literature since the turn of the century.<sup>1</sup> From this renewed interest in the discovery and development of powerful new solvents for difficult to dissolve polymeric bio-solutes, protic “*superbase*” ILs have emerged as promising candidates for cellulose dissolution and upstream processing related to a variety of materials.<sup>2–8</sup> To date, focus in the literature has largely been bounded by efforts to identify liquid salts with qualitative dissolution utility for biomass components, among various contributions detailing new developments in synthetic carbohydrate derivatisation chemistry.<sup>9,10</sup> Much less attention has been given towards gaining a detailed understanding of the energetics governing *solvent-solute* contact-encounters in such mixtures, using robust thermodynamic methods.<sup>11</sup>

Knowledge gained from such approaches reveal available composition- and temperature-dependent solvation character of both solvent-*j* and solute-*i*, which in turn provides the fundamental basis upon which the solvent selection process may be anchored, and furthermore, the means to identify a given solvent’s utility in terms of *true* task specificity. Herein, we report thermodynamic solution behaviour of cellulose dissolved in the superbase comprised IL, [m-TBDH][AcO] (7-methyl-1,5,7-triazabicyclo[4.4.0]dec-5-enium acetate). Employing a minimal experimental data set, we present the subsequent processing and interpretation of results obtained directly from

fundamental thermodynamic relationships, thereby avoiding various well-known limitations introduced by numerous thermodynamic polymer models available (*e.g.* Flory–Huggins and associated theoretical developments).<sup>12–17</sup>

This investigation relies on the well-known colligative property defined by the freezing point depression of the solvent-*j*, in the presence of solute-*i*, at low mass fractions,  $w_i$ . In combination with the Gibbs–Duhem relation for a 2 component system,  $w_i \text{dln}(a_i) + w_j \text{dln}(a_j) = 0$ , this permits the realisation of solute-*i* activities ( $a_i$ ) based on those experimentally determined for the solvent-*j* ( $a_j$ ). In essence, freezing point depressions for the binary solutions, recorded experimentally using modulated differential scanning calorimetry (MDSC), reveal changes to  $a_j$  using the variant of Kirchhoff’s law given in eqn (1), imposed by the presence of solute-*i* (*i.e.* enocell-*i*)<sup>‡</sup>, which perturbs the chemical potential of the solvent-*j*, [m-TBDH][AcO]-*j*, to a measurable extent.

$$\ln(a_j(T)) = \frac{H_{\text{fus.}} - \Delta C_p T_{\text{fus.}}}{RT} \left( \frac{T_{\text{fus.}}}{T} - 1 \right) - \frac{\Delta C_p}{R} \ln \left( \frac{T_{\text{fus.}}}{T} \right) - \frac{\Delta V}{RT} (P - P_{\text{fus.}}) \quad (1)$$

Scaling of solvent activities,  $a_j$ , based on the depressed freezing temperature  $T$ , obtained from eqn (1), to temperatures of interest,  $T'$ , was accomplished using the variant of the Gibbs–Helmholtz relation given in eqn (2),

$$R \text{dln}(a_j) = - \frac{\bar{H}_j}{T^2} \text{d}T \quad (2)$$

Materials Chemistry Division, Department of Chemistry, University of Helsinki, P. O. Box 55, FI-00014, Finland. E-mail: gordon.driver@helsinki.fi; gordon.driver@gmail.com; Tel: +358 50 593 9238

<sup>†</sup> Electronic supplementary information (ESI) available: Experimental data are reported along with the methods employed. See DOI: 10.1039/d0ra08892g

<sup>‡</sup> Enocell starting material:  $\text{DP}_n = 333$  and  $\text{DP}_w = 1333^9$



**Table 1** Experimentally determined thermodynamic quantities for binary mixtures of enocell-i and [m-TBDH][AcO]-j – variation of mass fraction,  $w_i$ , at constant temperature 360.15 K

$w_i$	$G_{\text{mix}}/\text{kJ mol}^{-1}$	$w_i H_i^E/\text{kJ mol}^{-1}$	$w_j H_j^E/\text{kJ mol}^{-1}$	$-TS_{\text{mix}}^b/\text{kJ mol}^{-1}$	$\Omega_i$	$\Omega_j$	$a_i$	$a_j$
0.00841	0.378	-0.759	-13.0	14.1	1.28	1.19	0.00208	1.18
0.0186	0.243	-1.92	-11.7	13.8	1.52	1.18	0.00785	1.16
0.115	-0.258	-27.4	-5.20	32.3	4.57	1.11	0.174	0.986

$$^a w_i H_i^E = H_{\text{mix}} - w_j H_j^E. \quad ^b -TS_{\text{mix}} = -T(S^{\text{ideal}} + S^E).$$

where  $\bar{H}_j$  represents the *relative* partial molar enthalpy of solvent-j. The Gibbs–Duhem relation, utilised on the basis of the form given in eqn (3),

$$\ln\left(\frac{a_i}{w_i}\right) = -\frac{w_j}{w_i} \int_{w_i=0}^{w_i=w} d\ln\left(\frac{a_j}{w_j}\right) \quad (3)$$

was subsequently employed to access, and verify, the thermodynamic consistency of desired excess thermodynamic quantities of solute-i.<sup>18</sup>

Freezing point depressions recorded during the independently run triplicate MDSC experiments produced standard deviations for a given composition on the order of  $\pm < 0.18$  K. Solute-i activity coefficients,  $\Omega_i$ , determined from experimentally recorded solvent-j activity coefficients,  $\Omega_j = \left(\frac{a_j}{w_j}\right)$ , via eqn (3), were subsequently employed to back-calculate experimentally determined values, again using eqn (3). The closeness of computed  $\Omega_j$ , obtained using  $\Omega_i$ , to the experimental values, serves as a consistency check, to validate and verify the  $\Omega_i$  obtained. We observed very satisfactory consistency by this method, where differences between experimental and calculated  $\Omega_j$  were generally  $\ll 1\%$  for dilute solutions, and up to  $\sim 5\%$  for certain  $w_j$ , at the highest temperature investigated (see the ESI†).

Selected thermodynamic results presented in Tables 1 and 2 are discussed below in terms of the thermodynamic suitability of [m-TBDH][AcO] for the task of dissolving cellulose, based on the molar Gibbs mixing energies, in relation to associated partial molar enthalpic and entropic contributions.<sup>§</sup>

Results presented in Table 1 indicate the presence of enocell-i in the dilute mixtures appears to impart a weak destabilising influence on the solvent-j where  $a_j > 1$  although this reverses with  $a_j < 1$  for the largest  $w_i$ , where  $a_i$  becomes substantial. Mixing becomes increasingly favourable with increases in  $w_i$ , where associated relative incremental changes to  $G_{\text{mix}}$  are observed to approach  $0 \text{ kJ mol}^{-1}$  from the positive side, crossing over to negative values for the 11.5 wt% enocell-i composition, where  $H_{\text{mix}} + -TS_{\text{mix}} < 0$ . As  $w_i$  increases from conditions of *infinite-dilution*, with *maximum* non-ideality due the absence of solute–solute contact-encounters, it becomes clear that such interactions, being attractive in nature, impart a favourable influence towards dissolution. Exclusion volumes, initially maintained *via* random polymer coiling (*e.g.* chain twisting and

kinking) at the lower mass fractions, reduce proportionally with subsequent increases in  $w_i$ , which serves to progressively stabilise the mixture. This effect materialises from an increase in permitted non-random (directional) contacts whereby solvent ions progressively access the polymer's coiled domain, as de-coiling proceeds due to polymer chain elongation.<sup>19</sup> Polymer de-coiling is further evidenced by conformational changes resulting in loss of degrees of freedom according to  $S_i^E = -77.5 \text{ J K}^{-1} \text{ mol}^{-1}$ .<sup>20</sup> Such an effect also influences the solvent-j albeit to a smaller extent with  $S_j^E = -15.2 \text{ J K}^{-1} \text{ mol}^{-1}$ , suggesting a lowering of solvent density (*c.f.* Table 2).<sup>21</sup> Such entropic contributions indicate directly the solvation character of enocell dissolved in [m-TBDH][AcO] and are expected to correlate with possible property enhancements observed with chemical modification chemistries, as well as with regeneration processes for different materials.<sup>22,23</sup> Polymer swelling, an unavoidable consequence of increased solvent penetration into the coiled domain, is rationalised here as serving to promote increased linearity of solvated polymer units, in proportion to degrees of freedom lost, enabling enhancement of their ability towards independent solution behaviour.

Across solute-i mass fractions,  $w_i$ , enthalpic stabilisation occurs, promoting dissolution, where  $H_{\text{mix}}$ , already strongly negative at the highly diluted compositions, more than doubles in the most concentrated composition. The magnitude of  $w_i H_i^E$ , at the investigated compositions, indicate attractive interactions of solute-i, with solvent-j, are strong and directional (*e.g.*  $i_j \neq j_i$  and with opposing composition dependence), revealing specific *attractive* solute–solvent contact-encounters driving dissolution, exceed contributions expected from random statistical solute–solvent contact-encounters characterised by  $-TS_{\text{mix}}$ . Simultaneous and progressive loss of  $w_j H_j^E$ , over the same composition range, indicate specific, directional solvent–solute contact configurations, that provide excellent stabilisation of the solute, are weakly less energetically favourable for the solvent. This opposing behaviour is facilitated by the large negative molar enthalpy of mixing at  $w_i = 0.115$ ,  $H_{\text{mix}} = -32.6 \text{ kJ mol}^{-1}$ , comprised of contributions due to enthalpic gains of  $w_i H_i^E$  that far outweigh contributions resultant from enthalpic losses exhibited by  $w_j H_j^E$ .

With the operative temperature range employed in this study being necessarily narrow, from  $\sim 7^\circ$  above the melting point of the solvent ( $\text{mp} = 350.34 \text{ K} \pm 1.44 \text{ K}$ ) to 373.15 K, we observe a near doubling of  $+G_i^E$  over the interval 357.15 K to 360.15 K at  $w_i = 0.115$ , to a value of  $0.521 \text{ kJ mol}^{-1}$ , a 43% increase, as repulsive forces increasingly dominate. Over the same

§ Further details of this method are provided in the available ESI.



**Table 2** Experimentally determined molar and partial molar Gibbs energies and partial molar entropy of mixing for a binary mixture of enocell-i and *[m*-TBDH][AcO]-j – variation of temperature at constant mass fraction  $w_i = 0.115$  (11.5 wt% enocell-i solution)

<i>T</i> /K	$G_{\text{mix}}^a/\text{kJ mol}^{-1}$	$G_i^{\text{ideal}}/\text{kJ mol}^{-1}$	$G_j^{\text{ideal}}/\text{kJ mol}^{-1}$	$G_i^E/\text{kJ mol}^{-1}$	$G_j^E/\text{kJ mol}^{-1}$	$\Omega_i$	$\Omega_j$
357.15	−0.527	−0.737	−0.320	0.296	0.234	2.39	1.09
358.15	−0.457	−0.739	−0.321	0.351	0.252	2.80	1.10
359.15	−0.369	−0.742	−0.322	0.425	0.269	3.46	1.11
360.15	−0.258	−0.744	−0.323	0.521	0.286	4.57	1.11
363.07 <sup>b</sup>	$8.82 \times 10^{-4}$	−0.750	−0.325	0.742	0.334	8.53	1.13
373.15	0.898	−0.770	−0.334	$1.52 \times 10^3$	0.480	72.3	1.19
$S_i^{\text{ideal}}/\text{J K}^{-1} \text{mol}^{-1}$		$S_j^{\text{ideal}}/\text{J K}^{-1} \text{mol}^{-1}$		$S_i^E/\text{J K}^{-1} \text{mol}^{-1}$		$S_j^E/\text{J K}^{-1} \text{mol}^{-1}$	
2.07		0.896		−77.5		−15.2	

<sup>a</sup>  $G_{\text{mix}} = G^{\text{ideal}} + G^E$ . <sup>b</sup> LCST = 363.127 K.

temperature range,  $+G_j^E$  increases by 18%. At yet higher temperatures, solute–solvent de-mixing becomes feasible as  $G_{\text{mix}} > 0$ , a result of the increasing magnitude of repulsive forces characterised by  $G^E$  as it effectively dominates the  $-TS^{\text{ideal}}$  term, for both solute-j and solvent-i. Enthalpic gains contributing to solvation are all but completely cancelled by the  $-TS_{\text{mix}}$  term, due to  $S_i^E$  being large and negative, signifying a loss of disorder that serves to disfavour dissolution, as indicated above. Such high temperature *de-mixing* behaviour is due to a type-V lower critical solution temperature (LCST), according to the classification scheme of Scott and van Konynenburg.<sup>24</sup> This result in an ionic liquid is bound to originate as a consequence of the increased ionicity of solvent ions, proportional to increased temperatures, where stabilising configurations for anion-solute, cation-solute and cation-anion interactions are lost due to thermal scattering and breaking of hydrogen bond interactions.<sup>25</sup> This expected behaviour is known to be controlled by oppositely charged ion dynamics as ions escape the potential energy wells of their nearest ionic neighbours, resulting in concomitant losses of the binding coulombic energy.<sup>26</sup>

Thermodynamic analyses presented indicate enocell-i solutions in *[m*-TBDH][AcO]-j are *non-ideal*, exhibiting positive deviations from Raoult's law, as observed by the sign of  $G_{i,j}^E$ . These solutions classify as *irregular*, with strong negative enthalpic contributions driving dissolution. Evolution of an increasingly large and positive  $-TS_{\text{mix}}$  term, due to polymer chain deformation of the Gaussian random coil and subsequent solvent ordering through the direct solute-ion contacts, induce a type-V LCST.<sup>20</sup> Accordingly, *[m*-TBDH][AcO] is well suited for the task of wood pulp dissolution, driven by strongly negative directional enthalpic contributions to solvation in the available temperature range below the LCST. Above  $T = 363.127$  K (for  $w_i = 0.115$ ), repulsive interactions between solute and solvent dominate to the extent that de-mixing instability is expected in the liquid phase, where increased temperatures will cease to benefit solution character. In this way, location of a LCST phase region must clearly be identified to ensure polymer dissolution is profitably carried out at appropriate temperatures. The Flory–Huggins model is, through its fundamental premise,

inappropriate for modelling of the title systems, in which the requirement for  $S_{\text{mix}} > 0$  is not met. Entropic effects leading to the expectation of a LCST may correlate with reported enhancement of material properties from use of ionic liquid solutions, suggesting dissolution temperatures in close proximity, yet below the LCST, are beneficial for chemical modification chemistries and regeneration processes.

## Conflicts of interest

There are no conflicts to declare.

## Notes and references

- R. P. Swatloski, S. K. Spear, J. D. Holbrey and R. D. Rogers, *J. Am. Chem. Soc.*, 2002, **124**, 4974–4975.
- A. M. Stepan, A. Michud, S. Hellstén, M. Hummel and H. Sixta, *Ind. Eng. Chem. Res.*, 2016, **55**, 8225–8233.
- L. K. J. Hauru, M. Hummel, K. Nieminen, A. Michud and H. Sixta, *Soft Matter*, 2016, **12**, 1487–1495.
- X. Li, H. Li, Z. Ling, D. Xu, T. You, Y.-Y. Wu and F. Xu, *Macromolecules*, 2020, **53**, 3284–3295.
- X. Niu, S. Huan, H. Li, H. Pan and O. J. Rojas, *J. Hazard. Mater.*, 2021, **402**, 124073.
- L. Jin, J. Gan, L. Cai, Z. Li, L. Zhang, Q. Zheng and H. Xie, *Polymers*, 2019, **11**, 994.
- T. Kakko, A. W. T. King and I. Kilpeläinen, *Cellulose*, 2017, **24**, 5341–5354.
- S. Elsayed, S. Hellsten, C. Guizani, J. Witos, M. Rissanen, A. H. Rantamäki, P. Varis, S. K. Wiedmer and H. Sixta, *ACS Sustain. Chem. Eng.*, 2020, **8**, 14217–14227.
- D. R. del Cerro, T. V. Koso, T. Kakko, A. W. T. King and I. Kilpeläinen, *Cellulose*, 2020, **27**, 5545–5562.
- S. Asaadi, T. Kakko, A. W. King, I. Kilpeläinen, M. Hummel and H. Sixta, *ACS Sustain. Chem. Eng.*, 2018, **6**, 9418–9426.
- J.-M. Andanson, A. A. H. Pádua and M. F. Costa Gomes, *ChemComm*, 2015, **51**, 4485–4487.
- P. J. Flory, *J. Chem. Phys.*, 1942, **10**, 51–61.
- M. L. Huggins, *J. Chem. Phys.*, 1941, **9**, 440.



- 14 J. M. Prausnitz, R. N. Lichtenthaler and E. Gomes de Azevedo, *Molecular Thermodynamics of Fluid-Phase Equilibria*, Prentice Hall, New Jersey, 3rd edn., 1999.
- 15 J. Gmehling, B. Kolbe, M. Kleiber and J. Rarey, *Chemical Thermodynamics for Process Simulation*, Wiley-VCH, Weinheim, 2012.
- 16 S. I. Sandler, *Chemical, Biochemical, and Engineering Thermodynamics*, John Wiley & Sons, New Jersey, 4th edn., 2006.
- 17 J. M. G. Cowie and V. Arrighi, *Polymers: Chemistry and Physics of Modern Materials*, Taylor & Francis, Boca Raton, 3rd edn., 2007.
- 18 M. L. Lakhanpal and B. E. Conway, *Can. J. Chem.*, 1960, **38**, 199–203.
- 19 P. C. Hiemenz, *Polymer Chemistry: The Basic Concepts*, Marcel Dekker, New York, 1984.
- 20 S. Seiffert, *Physical Chemistry of Polymers: A Conceptual Introduction*, De Gruyter, Berlin, 2020.
- 21 P. Paricaud, A. Galindo and G. Jackson, *Mol. Phys.*, 2003, **101**, 2575–2600.
- 22 H. Sixta, A. Michud, L. Hauru, S. Asaadi, Y. ma, A. King, I. Kilpeläinen and M. Hummel, *Nord. Pulp Pap Res. J.*, 2015, **30**, 43–57.
- 23 B. Kosan, C. Michels and F. Meister, *Cellulose*, 2008, **15**, 59–66.
- 24 P. H. van Konynenburg, R. L. Scott and J. S. Rowlinson, *Philos. Trans. Royal Soc. A*, 1980, **298**, 495–540.
- 25 G. W. Driver, Y. Huang, A. Laaksonen, T. Sparrman, Y.-L. Wang and P.-O. Westlund, *Phys. Chem. Chem. Phys.*, 2017, **19**, 4975–4988.
- 26 G. W. Driver, PhD thesis, The Queen's University of Belfast, 2007.

